Charrett, T.O.H. and Tatam, R.P. 2015. Objective speckle displacement resulting from the deformation of shaped objects. Proceedings of the SPIE, 9525, Optical measurement systems for industrial inspection IX, paper number 95251N. DOI: 10.1117/12.2184060

Objective speckle displacement resulting from the deformation of shaped objects.

Thomas O.H. Charrett*[a], Ralph P. Tatam [a]
[a] Engineering Photonics, Cranfield University, Cranfield, MK43 0AL, United Kingdom;
*t.charrett@cranfield.ac.uk

ABSTRACT

This paper describes an extended theory of the displacement of the objective speckle pattern resulting from displacement and/or deformation of a coherently illuminated diffuse object where the influence of the surface shape is included via the linear surface gradients. An experimental system capable of measuring the translational scaling factors, the ratios of speckle shift to object translations, to an accuracy of ± 0.02 and a repeatability of approximately ± 0.008 is described which was used to experimentally measure the speckle shift for a range of detector positions and surface gradients. The original expressions developed by Yamaguchi[1] and the new extended expressions[2] are then compared with experimental results for measurements on zero surface gradients, i.e. the mean surface lying in the x-y plane. The divergence of Yamaguchi's expressions from experimental results for off-axis detector positions that was first observed by Světlík[3] was confirmed, and the new expressions shown to successfully predict translational scaling factors for off-axis positions. The new expressions are then compared to the experimental results for a range of surface gradient magnitudes and directions, as well as detector positions both on and off-axis, and shown to successfully predict the observed speckle shift.

Keywords: laser speckle, correlation, metrology, instrumentation

1. INTRODUCTION

In many areas of non-contact optical measurement the properties of laser speckle are of great interest in particular in the measurement technique termed laser speckle pattern correlation[1] where the deformation of an illuminated object is related to the translation and de-correlation of its observed speckle pattern. The method was first described in the 1980's by Yamaguchi[1], who applied it to the measurement of object translation, rotation and strain[4–6] and surface roughness[7]. More recently, there has been renewed interest in the technique with researchers investigating new applications in industry, including vibration[8], surface slope and topology measurements[9] and robotic vehicle odometry[10,11]. In many of these applications knowledge of how the illuminated surface shape affects the observed speckle translation is of fundamental importance. For example, in robotic vehicle velocimetry systems a shaped surface has been observed to cause significant errors in the measured velocities (see section 2). The expressions for the speckle shift that have been previously presented[1,3,12,13] have not addressed the cases of shaped or sloped objects, apart from cylindrical surfaces[5], although Yamaguchi[14] has also recently applied computer simulations in an attempt to model the speckle displacement from curved surfaces. This paper first presents results demonstrating the effect that surface shape can have in objective speckle correlation measurements using example data from a speckle velocimeter[11]. Then new extended expressions[2] with the surface shape included by means of the linear surface gradients are presented and the results of this extended theory compared to experimental measurements of the translational scaling factors (the ratios of speckle shift to object translations) for a variety of detector/source configurations and surface gradients.

2. OBSERVATION OF THE EFFECT OF SURFACE SHAPE IN SPECKLE VELOCIMETRY

From our recent work in applying speckle correlation to the velocimetry of space exploration rovers[10,11] it became apparent that the surface shape is an important source of errors, which in the case of a rover cannot be corrected as the surface terrain is unknown. For example Figure 1 shows the influence of the surface tomography on the velocity signal measured when a linear translation stage is used to translate an objective speckle velocimeter[11] across a range of surfaces at a constant speed of 50mm/s. Figure 1 (a) shows measurements made on smooth laboratory vinyl floor surface and a sandy surface strewn with small rocks (~10-50mm in dimension), here the fluctuations about the translation mean stage speed can be seen, with the standard deviation increasing from 2.1mm/s to 2.6mm/s, although the signal is dominated by

the stage vibrations the additional error is predominantly due to the influence of surface shape changing the magnitude of the speckle displacement. In Figure 1 (b) a more controlled test was performed using a cardboard ramp consisting of a 30° incline, an upper platform at z=30mm, and a 30° decline. Here the signal was recorded using a lower stage speed to reduced stage vibrations, and at a higher data rate to allow temporal filtering (kernel of length = 100 samples = 0.4ms). This allows the underlying change in the measured velocity to be clearly seen, without being masked by stage vibrations or random measurement noise. It can be seen that the magnitude of the measured velocity drops when the laser spot is traversing the up-ramp, before returning to approximately the same value when on the upper platform, the slight remaining difference here can be accounted for by the changing in working distance (+30mm) of the velocimeter from the surface. On the down-slope the measured velocity can be been seen to increase before returning the original value for traversing the floor surface. It can be seen that the magnitude of this effect can be large, from Figure 1 (b) ~±3.5% of the actual velocity, therefore to better understand the technique and how a speckle velocimeter can be optimized the theory described in section 3 below was developed.

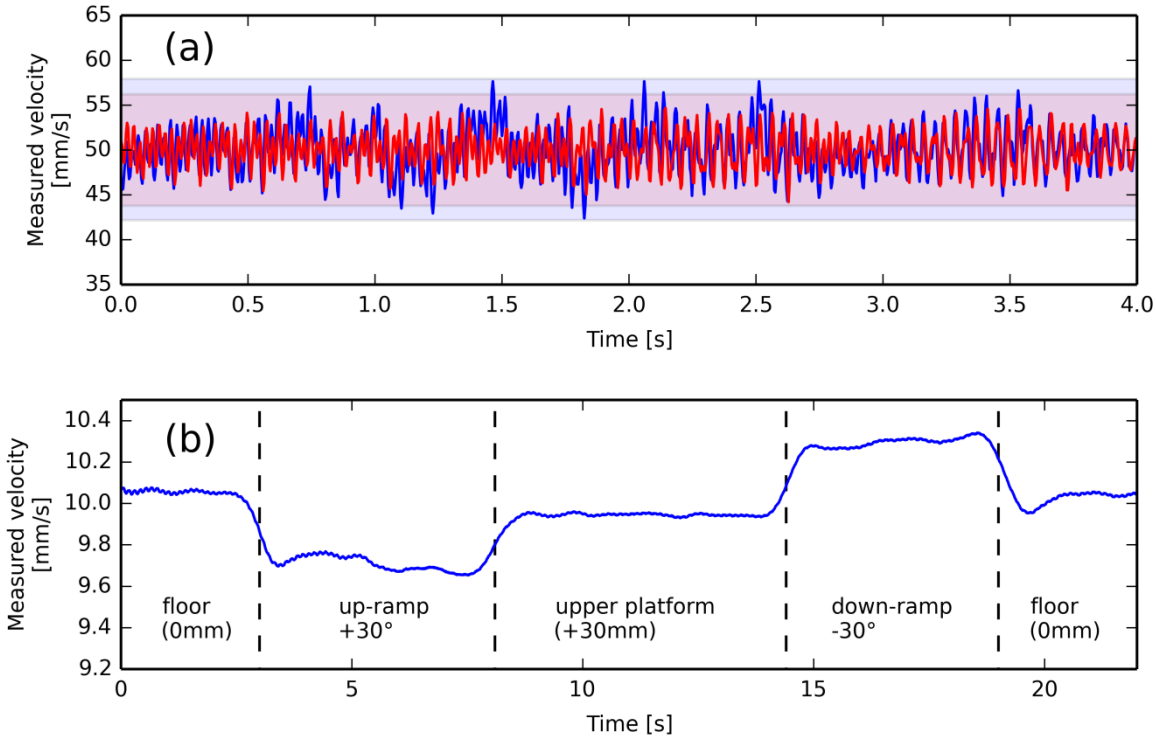

Figure 1. Influence of surface topography on the signal from an objective speckle velocimeter.

(a) The measured velocity using an objective speckle velocimeter mounted on a linear translation stage moves above different surfaces at a constant velocity of 50mm/s (red) a laboratory vinyl floor and (blue) sand with small rocks ~10-50mm in dimension, the shaded regions show the ±3 standard deviation range in the signals for the two surfaces.

(b) The measured velocity when traversing a 30^{o} ramp at 10mm/s. Here the signal has been filtered with a kernel of length = 100 samples = 0.4ms to reduce the random error and stage vibrations to allow the underlying change in measured velocity to be seen.

3. EXTENDED THEORY FOR THE SPECKLE SHIFT FROM SHAPED SURFACES

In this section we present a brief derivation of the extended theory for the speckle shift from shaped objects where a full derivation and comparison with previous methods can be found in[2]. The geometry of a speckle correlation experiment using objective speckle can be described by Figure 2, while the symbols used in the derivation can found in table 1. Where a light source located at $\boldsymbol{S}$, illuminates the point $\boldsymbol{R}$ on the mean object surface, and the objective speckle pattern is observed by a detector at point $\boldsymbol{D}$ located at $z = L_0$.

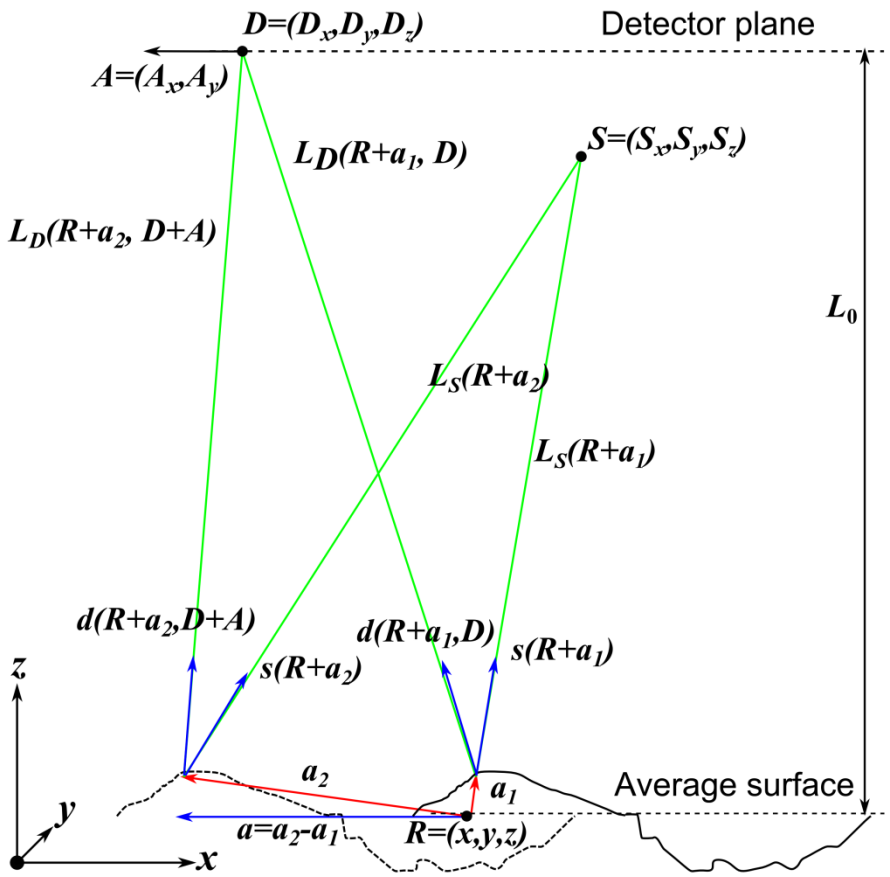

Figure 2. General representation of the geometry used in the development of the speckle shift theory via cross-correlation of speckle intensities.

The intensity observed at the detector is given, in terms of the complex amplitude of the scattered light, $U(\boldsymbol{D})$, by $I(\boldsymbol{D})=|U(\boldsymbol{D})|^2$ and the complex amplitudes of the scattered light before, $U_1(\boldsymbol{D}_1)$ and after deformation or displacement, $U_2(\boldsymbol{D}_2)$ can be written in terms of the path lengths as [1]:

$$U_n(\boldsymbol{D}_n)=\iint\sqrt{I_0\left(\boldsymbol{R}+\alpha_{Tn}(\boldsymbol{R})\right)}\zeta(\boldsymbol{R})\exp(i\phi) \times\exp\left(ik\left[\left|\boldsymbol{L}_S(\boldsymbol{R})-\boldsymbol{a}_n(\boldsymbol{R})\right|+\left|\boldsymbol{L}_D(\boldsymbol{R},\boldsymbol{D}_n)-\boldsymbol{a}_n(\boldsymbol{R})\right|\right]\right)dxdy \quad (1)$$

Where $n=1,2$, the vectors, $\boldsymbol{L}_s(\boldsymbol{R})$ and $\boldsymbol{L}_D(\boldsymbol{R},\boldsymbol{D}_n)$ point from the mean object surface $\boldsymbol{R}$ to the light source $\boldsymbol{S}$ and observation point $\boldsymbol{D}_n$ respectively. The vector representing the displacement of the actual scattering surface from the mean object surface is given by $\boldsymbol{a}_n(\boldsymbol{R})$ and $I_0\left(\boldsymbol{R}+\alpha_{Tn}(\boldsymbol{R})\right)$ represents the intensity of the illuminating light at the surface point, where $\alpha_{Tn}(\boldsymbol{R})$ is the projection of $\boldsymbol{a}_n(\boldsymbol{R})$ onto the *x*-*y* plane. $\zeta(\boldsymbol{R})$ and $\exp(i\phi)$ are the macroscopic and microscopic reflection functions of the object and are related to the diffusing properties of the object[1] and k is the wavenumber.

Table 1. Notation used in derivation of expressions relating the deformation and translation of a shaped surface to the shift in the speckle pattern.

Symbol	Description
$\boldsymbol{S}$	Source position vector
$\boldsymbol{D}$	Detector position vector
$\boldsymbol{R}$	Position vector of the illuminated point on mean surface
$U(\boldsymbol{D})$	Complex amplitude at detector
$I(\boldsymbol{D}) = \lvert U(\boldsymbol{D})\rvert^2$	Intensity at detector
$\boldsymbol{a_n(R)} = (a_x, a_y, a_z)$	Displacement of point $\boldsymbol{R}$ from the mean surface
$\alpha_{Tn}(\boldsymbol{R})$	the projection of $\boldsymbol{a_n(R)}$ onto the *x*-*y* plane
k	Optical wavenumber
$\boldsymbol{A} = (A_x, A_y, 0)$	Vector to shifted speckle pattern in the x-y plane at the detector.
$\boldsymbol{a}(\boldsymbol{R}) = \boldsymbol{a_2}(\boldsymbol{R}) - \boldsymbol{a_1}(\boldsymbol{R})$	The surface translation vector at point $\boldsymbol{R}$.
$\boldsymbol{L_S}(\boldsymbol{R})$	Vector from $\boldsymbol{S}$ to $\boldsymbol{R}$
$\boldsymbol{L_D}(\boldsymbol{R}, \boldsymbol{D})$	Vector from $\boldsymbol{R}$ to $\boldsymbol{D}$
$\boldsymbol{s(R)} = (s_x, s_y, s_z)$, $L_S(\boldsymbol{R})$	Unit vector and magnitude of $\boldsymbol{L_S}(\boldsymbol{R})$
$\boldsymbol{d(R, D)} = (d_x, d_y, d_z)$, $L_D(\boldsymbol{R}, \boldsymbol{D})$	Unit vector and magnitude of $\boldsymbol{L_D}(\boldsymbol{R},\boldsymbol{D})$
$\boldsymbol{p}(\boldsymbol{R}, \boldsymbol{D}) = \boldsymbol{s}(\boldsymbol{R}) + \boldsymbol{d}(\boldsymbol{R}, \boldsymbol{D})$	Substitution used in derivation.

An expression for the speckle shift resulting from a small object translation/deformation is then found from the cross-correlation function of the scattering intensities $I_1(\boldsymbol{D_1})$ and $I_2(\boldsymbol{D}_2)$ at instances before and after the deformation which can be written as:

$$\left\langle I_1(\boldsymbol{D_1}) I_2^*(\boldsymbol{D_2}) \right\rangle = \left\langle \left|U_1(\boldsymbol{D_1})\right|^2 \right\rangle \left\langle \left|U_2(\boldsymbol{D}_2)\right|^2 \right\rangle + \left| \left\langle U_1(\boldsymbol{D_1}) U_2^*(\boldsymbol{D_2}) \right\rangle \right|^2 \tag{2}$$

However, only the second term in (2) is of interest in determining the speckle shift, as this represents the cross-correlation function of the fluctuation of the intensity about the mean, i.e. the speckles. If the detector is originally located at $\boldsymbol{D_1} = \boldsymbol{D}$ then the maximum of this term will occur at the shifted detector position that corresponds to the speckle shift $\boldsymbol{A}$, hence $\boldsymbol{D_2} = \boldsymbol{D} + \boldsymbol{A}$. As in Yamaguchi's original derivation we also set $\alpha_{T1}(\boldsymbol{R}) = 0$, the surface translation vector, $\boldsymbol{a}(\boldsymbol{R}) = \boldsymbol{a_2}(\boldsymbol{R}) - \boldsymbol{a_1}(\boldsymbol{R})$. Finally, the paths from the source to surface-point, $\left|\boldsymbol{L_S}(\boldsymbol{R}) - \boldsymbol{a_n}(\boldsymbol{R})\right|$ and surface-point to observation points, $\left|\boldsymbol{L_D}(\boldsymbol{R}, \boldsymbol{D_n}) - \boldsymbol{a_n}(\boldsymbol{R})\right|$ before and after the deformation can be approximated by:

$$\begin{aligned}
&\left|\boldsymbol{L_S}(\boldsymbol{R}) - \boldsymbol{a}_1(\boldsymbol{R})\right| \approx L_S(\boldsymbol{R}) - \boldsymbol{a}_1(\boldsymbol{R}) \cdot \boldsymbol{s}(\boldsymbol{R}) \\
&\left|\boldsymbol{L_S}(\boldsymbol{R}) - \boldsymbol{a}_2(\boldsymbol{R})\right| \approx L_S(\boldsymbol{R}) - \boldsymbol{a}_2(\boldsymbol{R}) \cdot \boldsymbol{s}(\boldsymbol{R}) \\
&\left|\boldsymbol{L}_D(\boldsymbol{R}, \boldsymbol{D}) - \boldsymbol{a}_1(\boldsymbol{R})\right| \approx L_D(\boldsymbol{R}, \boldsymbol{D}) - \boldsymbol{a}_1(\boldsymbol{R}) \cdot \boldsymbol{d}(\boldsymbol{R}, \boldsymbol{D}) \\
&\left|\boldsymbol{L}_D(\boldsymbol{R}, \boldsymbol{D} + \boldsymbol{A}) - \boldsymbol{a}_2(\boldsymbol{R})\right| \approx L_D(\boldsymbol{R}, \boldsymbol{D}) - \boldsymbol{a}_2(\boldsymbol{R}) \cdot \boldsymbol{d}(\boldsymbol{R}, \boldsymbol{D}) + \boldsymbol{A} \cdot \boldsymbol{d}(\boldsymbol{R}, \boldsymbol{D})
\end{aligned} \tag{3}$$

Here, $\boldsymbol{s}(\boldsymbol{R})$ and $\boldsymbol{d}(\boldsymbol{R},\boldsymbol{D})$ are unit vectors in the direction of $\boldsymbol{L_S}(\boldsymbol{R})$ and $\boldsymbol{L_D}(\boldsymbol{R},\boldsymbol{D})$ respectively and $L_S(\boldsymbol{R})$ and $L_D(\boldsymbol{R},\boldsymbol{D})$ are the magnitudes. Substituting these expressions, $\boldsymbol{p}(\boldsymbol{R}, \boldsymbol{D}) = \boldsymbol{s}(\boldsymbol{R}) + \boldsymbol{d}(\boldsymbol{R}, \boldsymbol{D})$ and setting $\alpha_{T1}(\boldsymbol{R}) = 0$ and $\boldsymbol{a_2}(\boldsymbol{R}) - \boldsymbol{a_1}(\boldsymbol{R}) = \boldsymbol{a}(\boldsymbol{R})$, the surface translation vector the following expression for the cross-correlation of the intensity fluctuations can be found:

$$\begin{aligned}
\left|\left\langle U_1(\boldsymbol{R}, \boldsymbol{D}) U_2^*(\boldsymbol{R}, \boldsymbol{D} + \boldsymbol{A})\right\rangle\right| = \iint &\sqrt{I_0(\boldsymbol{R}) I_0(\boldsymbol{R} + \alpha_{T2}(\boldsymbol{R}))} \\
&\times \exp\left(ik\left[\boldsymbol{p}(\boldsymbol{R}, \boldsymbol{D}) \cdot \boldsymbol{a}(\boldsymbol{R}) - \boldsymbol{A} \cdot \boldsymbol{d}(\boldsymbol{R}, \boldsymbol{D})\right]\right) dxdy
\end{aligned} \tag{4}$$

Taylor series expansions, about $\boldsymbol{R}$ = 0 and ignoring terms higher than first order, are then used to expand the $\boldsymbol{p}(\boldsymbol{R},\boldsymbol{D})\cdot\boldsymbol{a}(\boldsymbol{R})$ and $\boldsymbol{A}\cdot\boldsymbol{d}(\boldsymbol{R},\boldsymbol{D})$ terms in equation (4) giving:

$$\begin{aligned}\left|\left\langle U_1(\boldsymbol{R},\boldsymbol{D})U_2^*(\boldsymbol{R},\boldsymbol{D}+\boldsymbol{A})\right\rangle\right| &= \exp\left(ik\left[\boldsymbol{A}\cdot\boldsymbol{d}(0,\boldsymbol{D})-\boldsymbol{p}(0,\boldsymbol{D})\cdot\boldsymbol{a}(0)\right]\right)\\ &\times\iint\sqrt{I_0(\boldsymbol{R})I_0(\boldsymbol{R}+\alpha_{T2}(\boldsymbol{R}))}\\ &\times\exp\left(ik\begin{bmatrix}-A_x\left[\nabla d_x(\boldsymbol{R},\boldsymbol{D})\right]_0-A_y\left[\nabla d_y(\boldsymbol{R},\boldsymbol{D})\right]_0\\ +\left[\nabla\boldsymbol{p}(\boldsymbol{R},\boldsymbol{D})\cdot\boldsymbol{a}(\boldsymbol{R})\right]_0\end{bmatrix}\cdot\boldsymbol{R}\right)dxdy\end{aligned} \tag{5}$$

By examining this equation it can be seen that the cross-correlation will be a maximum where the exponential term is zero, hence:

$$\left[-A_x\left[\nabla d_x(\boldsymbol{R},\boldsymbol{D})\right]_0-A_y\left[\nabla d_y(\boldsymbol{R},\boldsymbol{D})\right]_0+\left[\nabla\boldsymbol{p}(\boldsymbol{R},\boldsymbol{D})\cdot\boldsymbol{a}(\boldsymbol{R})\right]_0\right]=0 \tag{6}$$

Which can be solved to give:

$$A_x=\frac{\frac{\delta d_y}{\delta y}\left(\frac{\delta\boldsymbol{p}\cdot\boldsymbol{a}}{\delta x}\right)-\frac{\delta d_y}{\delta x}\left(\frac{\delta\boldsymbol{p}\cdot\boldsymbol{a}}{\delta y}\right)}{\left(\frac{\delta d_x}{\delta x}\frac{\delta d_y}{\delta y}-\frac{\delta d_x}{\delta y}\frac{\delta d_y}{\delta x}\right)}\qquad A_y=\frac{\frac{\delta d_x}{\delta x}\left(\frac{\delta\boldsymbol{p}\cdot\boldsymbol{a}}{\delta y}\right)-\frac{\delta d_x}{\delta y}\left(\frac{\delta\boldsymbol{p}\cdot\boldsymbol{a}}{\delta x}\right)}{\left(\frac{\delta d_x}{\delta x}\frac{\delta d_y}{\delta y}-\frac{\delta d_x}{\delta y}\frac{\delta d_y}{\delta x}\right)} \tag{7}$$

Finally the $\frac{\delta\boldsymbol{p}\cdot\boldsymbol{a}}{\delta x}$ and $\frac{\delta\boldsymbol{p}\cdot\boldsymbol{a}}{\delta y}$ terms can be expanded in terms of the partial derivatives and components of the strain tensor and rotation vector, as in the original Yamaguchi derivation[1]:

$$\varepsilon_{xx}=\frac{\delta a_x}{\delta x},\qquad \varepsilon_{yy}=\frac{\delta a_y}{\delta y},\qquad \varepsilon_{xy}=\varepsilon_{yx}=\frac{1}{2}\left(\frac{\delta a_x}{\delta y}+\frac{\delta a_y}{\delta x}\right) \tag{8}$$

$$\Omega_x=\frac{\delta a_z}{\delta y},\qquad \Omega_y=-\frac{\delta a_z}{\delta x},\qquad \Omega_z=\frac{1}{2}\left(\frac{\delta a_y}{\delta x}+\frac{\delta a_x}{\delta y}\right) \tag{9}$$

When the surface shape is approximated by its linear surface gradients, $m_x=\delta z/\delta x, m_y=\delta z/\delta y$; and $\boldsymbol{S}=L_S(s_x,s_y,s_z)$, $\boldsymbol{D}=L_D(d_x,d_y,d_z)$ then $\boldsymbol{R}=\left(x,y,m_x x+m_y y\right)$ and the partial derivatives required in equation (7) above can be written as:

$$\begin{aligned}\frac{\delta\boldsymbol{s}}{\delta x}&=\frac{1}{L_S}\left(m_x s_x s_z+{s_x}^2-1,\quad m_x s_y s_z+s_x s_y,\quad m_x\left({s_z}^2-1\right)+s_x s_z\right)\\ \frac{\delta\boldsymbol{s}}{\delta y}&=\frac{1}{L_S}\left(m_y s_x s_z+s_x s_y,\quad m_y s_y s_z+{s_y}^2-1,\quad m_y\left({s_z}^2-1\right)+s_y s_z\right)\\ \frac{\delta\boldsymbol{d}}{\delta x}&=\frac{1}{L_D}\left(m_x d_x d_z+{d_x}^2-1,\quad m_x d_y d_z+d_x d_y,\quad m_x\left({d_z}^2-1\right)+d_x d_z\right)\\ \frac{\delta\boldsymbol{d}}{\delta y}&=\frac{1}{L_D}\left(m_y d_x d_z+d_x d_y,\quad m_y d_y d_z+{d_y}^2-1,\quad m_y\left({d_z}^2-1\right)+d_y d_z\right)\end{aligned} \tag{10}$$

Substituting these into equation (7) are rearranging to a matrix form similar to that used by Světlík[3] for compactness gives the final expressions:

$$\begin{bmatrix} Ax \\ Ay \end{bmatrix} = [P]\left(\left([T] + [T'] \right) \begin{bmatrix} a_x \\ a_y \\ a_z \end{bmatrix} + [R] \begin{bmatrix} \Omega_x \\ \Omega_y \\ \Omega_z \end{bmatrix} + [D] \begin{bmatrix} \varepsilon_{xx} \\ \varepsilon_{xy} \\ \varepsilon_{yy} \end{bmatrix} \right) \tag{11}$$

Where:

$$[P] = \frac{L_D}{\left({d_z}^2 - m_x d_x d_z - m_y d_y d_z \right)} \begin{bmatrix} \left(m_y d_y d_z + {d_y}^2 - 1 \right) & -\left(m_x d_y d_z + d_y d_x \right) \\ -\left(m_x d_x d_z + d_y d_x \right) & \left(m_x d_x d_z + {d_x}^2 - 1 \right) \end{bmatrix}$$

$$[T] = \begin{bmatrix} \frac{\left({s_x}^2 - 1 \right)}{L_S} + \frac{\left({d_x}^2 - 1 \right)}{L_D} & \frac{\left(s_x s_y \right)}{L_S} + \frac{\left(d_x d_y \right)}{L_D} & \frac{\left(s_x s_z \right)}{L_S} + \frac{\left(d_x d_z \right)}{L_D} \\ \frac{\left(s_x s_y \right)}{L_S} + \frac{\left(d_x d_y \right)}{L_D} & \frac{\left({s_y}^2 - 1 \right)}{L_S} + \frac{\left({d_y}^2 - 1 \right)}{L_D} & \frac{\left(s_y s_z \right)}{L_S} + \frac{\left(d_y d_z \right)}{L_D} \end{bmatrix}$$

$$[T'] = \begin{bmatrix} m_x \left(\frac{s_x s_z}{L_S} + \frac{d_x d_z}{L_D} \right) & m_x \left(\frac{s_y s_z}{L_S} + \frac{d_y d_z}{L_D} \right) & m_x \left(\frac{\left({s_z}^2 - 1 \right)}{L_S} + \frac{\left({d_z}^2 - 1 \right)}{L_D} \right) \\ m_y \left(\frac{s_x s_z}{L_S} + \frac{d_x d_z}{L_D} \right) & m_y \left(\frac{s_y s_z}{L_S} + \frac{d_y d_z}{L_D} \right) & m_y \left(\frac{\left({s_z}^2 - 1 \right)}{L_S} + \frac{\left({d_z}^2 - 1 \right)}{L_D} \right) \end{bmatrix}$$

$$[R] = \begin{bmatrix} 0 & -\left(s_z + d_z \right) & \left(s_y + d_y \right) \\ -\left(s_z + d_z \right) & 0 & -\left(s_x + d_x \right) \end{bmatrix}$$

$$[D] = \begin{bmatrix} \left(s_x + d_x \right) & \left(s_y + d_y \right) & 0 \\ 0 & \left(s_x + d_x \right) & \left(s_y + d_y \right) \end{bmatrix}$$

4. EXPERIMENTAL MEASUREMENT OF SPECKLE SCALING COOEFIECENTS

Experimental setup

To experimentally test the above relations, an experimental system was constructed using an aluminum profile support structure above a test object mounted on a translation stage (Physik Instrumente M-110.1DG linear translation stage with a quoted unidirectional repeatability of 0.1µm) positioned in the *xy*-plane at *z* = 0mm. The three-dimensional support structure allowed the positions of the laser source and camera to be varied over a wide range of geometries (~ ± 80mm in *x*,*y* and up to 400mm in *z*) that are typical of practical applications of the speckle correlation method such as speckle velocimetry[10,11]. The test objects used were custom 3D printed ramps with gradients of 0.0 (flat), 0.2, 0.4, 0.6, 0.8 and 1.0 (45° slope) as shown in Figure 3. The ramps were constructed with an octagonal cross-section allowing the gradients to be rotated in 45° increments to vary both components of the surface gradient in a controlled manner. The quoted precision of the 3D printing process was ± 0.1mm over a ramp dimension of 30mm giving a precision of the gradients of ± 0.003. The camera was a Baumer HXC-13 CMOS camera with 14x14µm pixels with a laser line filter located in front of the camera sensor to block background light and ensure high contrast speckle images. The laser source used was a diode-pumped solid state (DPSS) laser module producing approximately 30mW at 532nm. The collimated output of the laser was expanded onto the surface of the test object using an *f* = 45mm lens to produce a speckle size of around 5 pixels on the camera.

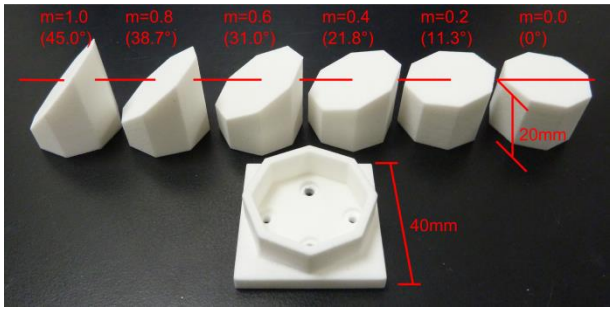

Figure 3. The 3D printed test objects used in this experiment. From left to right $m_{x,y}$ = 1.0, 0.8, 0.6, 0.4, 0.2 and 0.0 and the stage mounting plate. The ramps have a constant working height of 20mm above the stage at the centre point and can be rotated in 45° increments in the mounting plate to enable the surface gradient direction to be rotated in a controlled manner.

Method

The translational scaling factors (ratios of speckle shift to object translation), A_x/a_x, A_x/a_y, A_x/a_z and A_y/a_x, A_y/a_y, A_y/a_z, were experimentally measured by recording images before and after a series of known translations, computing the normalized cross-correlation[15] and applying Gaussian peak fitting[16] to determine the speckle shift to 0.1 pixel accuracy (1.4µm). Each translation was repeated 10 times and the mean shift recorded. This was performed from stage translation between 0 and 500µm to avoid the effects of pixel locking[16] and/or stage positional bias errors caused by unwanted stage roll, pitch or yaw. The final translational scaling factors were estimated to an accuracy of ± 0.02 using a linear fit to the recorded mean shift at each translation magnitude. The accuracy is limited by the ability to align the detector and stage axis, currently estimated at 0.5° by measurement of the length and transverse displacement possible when fixing the mounting brackets, any misalignment will cause translations in the other two orthogonal components, resulting in an unwanted contribution to speckle shift. This angular misalignment comes from both misalignment of the stage with the support structure, which is constant, and from misalignment of the camera and support structure which can vary each time the camera is repositioned. However although the accuracy of the scaling factors was limited to ± 0.02 the repeatability is approximately ± 0.008, and is limited by the pixel size of the detector and the 0.1 pixel peak fitting accuracy.

Results

For the case of zero surface gradients, the expressions derived in equation (11) reduce to expressions that are different to those given by Yamaguchi[1] and Horvath *et al.*[13]. However Světlík[3] derives expressions for the speckle shift using a different approach that agree with those found above and those found by Jacquot[12]. A comparison of the measured and theoretical translation scaling factors for this case is shown Figure 4(a). As the detector location is moved along the x-axis, away from the z-axis it can be seen that the experimental values diverge from the values predicted by Yamaguchi's expressions[1] (shown as dashed lines). This divergence from the theory was also noted by Světlík[3] and is most noticeable in the A_x/a_x, A_y/a_y components. The values predicted by the expressions derived above are shown in Figure 4 as the thick green line, where the thickness denotes the minimum and maximum bounds predicted assuming an error in source and detector positions of ± 1mm in all directions. These values successfully predict the observed translation scaling factors within the tolerances of the measurements (± 0.02) over a wide range of detector positions along the *x*-axis for this zero gradient case, confirming the results reported by Světlík[3].

The case of non-zero surface gradients can be seen in Figure 4 (b) and (c), and Figure 5. In Figure 4 (b) and (c) the change in the scaling factors with varying detector position can be seen to be in good agreement with the new expressions presented in section 3. Likewise in Figure 5 the dependence upon the surface gradient can be seen to be in good agreement for both changing magnitudes (a) and (b), and changing direction (c). Other detector positions within the range $x, y < \pm$ 80mm have also been investigated[2] and similarly found to be in agreement with the extended theory.

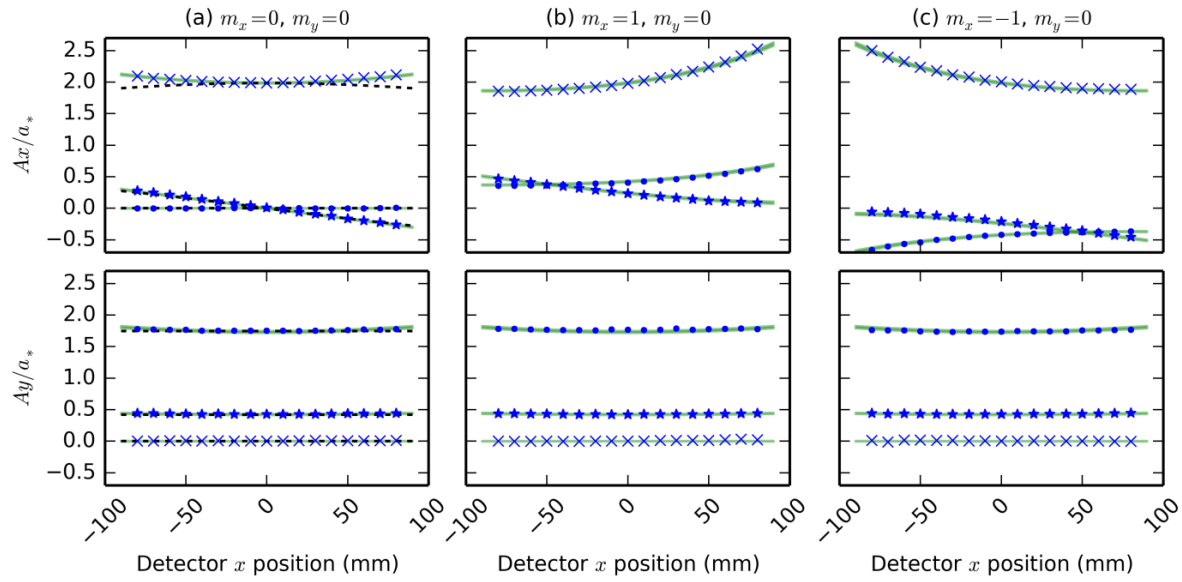

Figure 4. Comparison of translational scaling factors for $\boldsymbol{S}$ = (0,-150,265) mm and $\boldsymbol{D}$ = (D_x,0,300) mm, for three surface gradients (a) $m_x = m_y = 0$; (b) $m_x = +1$, $m_y = 0$ and (c) $m_x = -1$, $m_y = 0$. The top row shows the scaling factors for the speckle shift in the x direction (A_x) resulting from the object translations (a_x, a_y and a_z) while the bottom row shows scaling factors for the speckle shift in the y direction (A_y). The data points are the experimental results; (✖) $A_{x,y}/a_x$, (●) $A_{x,y}/a_y$ and (★) $A_{x,y}/a_z$, and the dashed lines in (a) show the values predicted by the Yamaguchi's equations (for $m_x = m_y = 0$). The solid lines (green) are the values predicted by the extended equations presented in section 3. Here the thickness of the line denotes the minimum and maximum bounds predicted assuming an error in source and detector positions of ± 1mm in all directions.

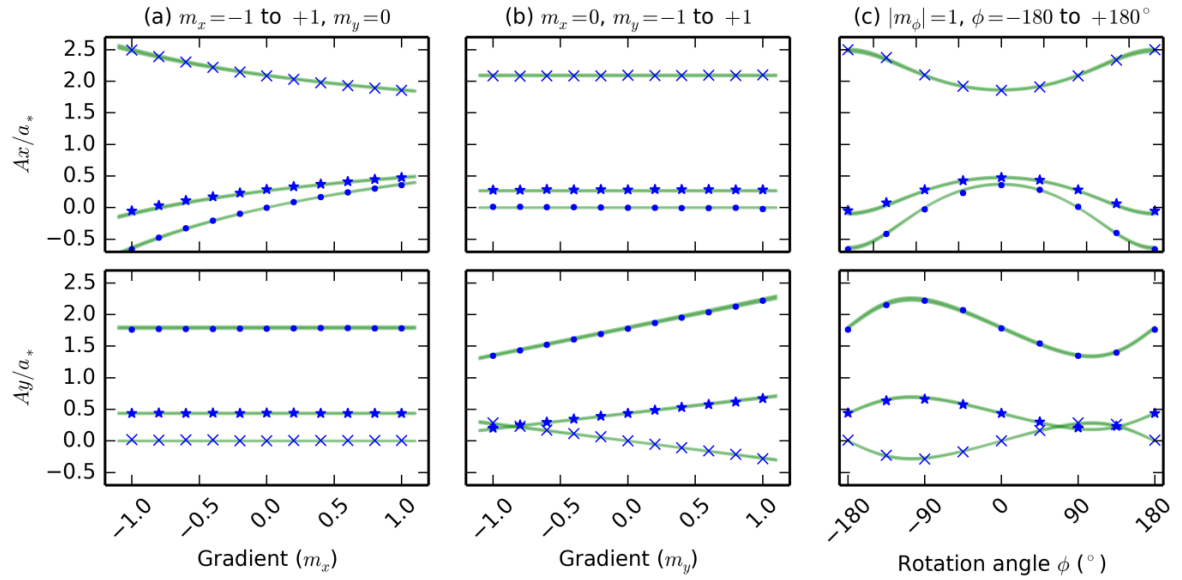

Figure 5. Comparison of translational scaling factors for $\boldsymbol{S}$ = (0,-150,265) mm and $\boldsymbol{D}$ = (–80,0,300) mm for (a) varying magnitude m_x; (b) varying magnitude m_y and (c) varying directions of a fixed magnitude gradient as it is rotated about the z-axis (m_x = cosϕ, m_y = -sinϕ). The top row shows the scaling factors for the speckle shift in the x direction (A_x) resulting from the object translations (a_x, a_y and a_z) while the bottom row shows scaling factors for the speckle shift in the y direction (A_y). The data points are the experimentally measured results; (✖)$A_{x,y}/a_x$, (●) $A_{x,y}/a_y$ and (★) $A_{x,y}/a_z$ and the solid lines show the values predicted by the extended equations (section 3). Here the thickness of the line denotes the minimum and maximum bounds predicted assuming an error in source and detector positions of ± 1mm in all directions.

5. CONCLUSIONS

The observation of a dependence on the speckle shift to surface shape has been shown to lead to significant errors in the application of the speckle correlation method in speckle velocimetry and is likely to be fundamental importance in other applications. Expressions relating the observed objective speckle shift to the deformation of the illuminated object have been presented and verified experimentally for shaped surfaces approximated by the linear surface gradients. The original expressions developed by Yamaguchi[1] and the new extended expressions are then compared with experimental results for measurements on zero surface gradients, i.e. the mean surface lying in the x-y plane. The divergence of Yamaguchi's expressions from experimental results for off-axis detector positions that was first observed by Světlík[3] was confirmed, and the new expressions shown to successfully predict translational scaling factors for off-axis positions. These new expressions are then compared to the experimental results for a range of surface gradient magnitudes and directions, as well as detector positions, both on and off-axis, and shown to successfully predict the observed speckle shift. This knowledge of how the speckle shift varies will be of great use for future improvements to speckle velocimetry, to reduce the sensitivity to the unknown surface gradient, and in the application of laser speckle correlation for industrial metrology on shaped objects to ensure high positional accuracy.

6. ACKNOWLEDGMENTS

The authors acknowledge the support of the Engineering and Physical Sciences Research Council (EPSRC) UK, via grant EP/H02252X/1 and EP/H019839/1. (For enquiries relating to access to the research data or other materials referred to in this article, please contact Cranfield University Library and Information Services – library@cranfield.ac.uk).

REFERENCES

[1] Yamaguchi, I., "Speckle Displacement and Decorrelation in the Diffraction and Image Fields for Small Object Deformation," Opt. Acta Int. J. Opt. **28**(10), 1359–1376 (1981).
[2] Charrett, T. O. H., Tatam, R. P., "Objective speckle displacement: an extended theory for the small deformation of shaped objects," Opt. Express **22**(21), 25466 (2014).
[3] Světlík, J., "Speckle Displacement: Two Related Approaches," J. Mod. Opt. **39**(1), 149–157 (1992).
[4] Yamaguchi, I., "Automatic measurement of in-plane translation by speckle correlation using a linear image sensor," J. Phys. E., **19**, 944-949, (1986).
[5] Yamaguchi, I.., Fujita, T., "Laser speckle rotary encoder," Appl. Opt. **28**(20), 4401–4406 (1989).
[6] Yamaguchi, I., "Advances in the laser speckle strain gauge," Opt. Eng. **27**(3), 214-218 (1988).
[7] Yamaguchi, I., Kobayashi, K.., Yaroslavsky, L., "Measurement of surface roughness by speckle correlation," Opt. Eng. **43**(11), 2753 (2004).
[8] Spagnolo, G. S., Paoletty, D.., Zanetta, P., "Local speckle correlation for vibration analysis," Opt. Commun. **123**, 41–48 (1996).
[9] Horváth, P., Šmíd, P., Wagnerova, P.., Hrabovský, M., "Usage of a speckle correlation for object surface topography," Proc. SPIE 6034, ICO20 Opt. Des. Fabr. **6034**, J. Breckinridge and Y. Wang, Eds., 603421–603421 – 6 (2006).
[10] Charrett, T. O. H., Waugh, L.., Tatam, R. P., "Speckle velocimetry for high accuracy odometry for a Mars exploration rover," Meas. Sci. Technol. **21**(2), 025301 (2010).
[11] Francis, D., Charrett, T. O. H., Waugh, L., Tatam, R. P., "Objective speckle velocimetry for autonomous vehicle odometry.," Appl. Opt. **51**(16), 3478–3490 (2012).
[12] Jacquot, P., Rastogi, P., "Speckle motions induced by rigid-body movements in freespace geometry: an explicit investigation and extension to new cases," Appl. Opt. **18**(12), 2022–2032 (1979).
[13] Horváth, P., Hrabovský, M.., Šmíd, P., "Full theory of speckle displacement and decorrelation in the image field by wave and geometrical descriptions and its application in mechanics," J. Mod. Opt. **51**(5), 725–742 (2004).
[14] Yamaguchi, I., "Speckle displacement for general object deformaton of a curved surface," Speckle 2012 V Int. Conf. Speckle Metrol. Proc. SPIE Vol. **8413**, Á. F. Doval and C. Trillo, Eds., 841307 (2012).
[15] Briechle, K., Hanebeck, U. D., "Template matching using fast normalized cross correlation," Proc. SPIE 4387, Opt. Pattern Recognit. XII, D. P. Casasent and T.-H. Chao, Eds., 95–102 (2001).
[16] Raffel, M., Willert, C., Wereley, S.., Kompenhans, J., Particle Image Velocimetry: a practical guide, Springer Berlin Heidelberg, Berlin, Heidelberg (2007).